Available online at www.sciencedirect.com
SCIENCE DIRECT®
Journal of Catalysis 221 (2004) 263–273
JOURNAL OF CATALYSIS
www.elsevier.com/locate/jcat

Active phase of Ni_2P/SiO_2 in hydroprocessing reactions

S.T. Oyama,* X. Wang, Y.-K. Lee, and W.-J. Chun

Environmental Catalysis and Materials Laboratory, Department of Chemical Engineering (0211), Virginia Polytechnic Institute and State University, Blacksburg, VA 24061, USA

Received 24 October 2002; revised 6 December 2002; accepted 23 December 2002

Abstract

A series of Ni_2P/SiO_2 catalyst samples with loading from 6 to 22 wt% Ni_2P was prepared by the method of temperature-programmed reduction (TPR). The samples were characterized by BET, CO uptake, X-ray diffraction (XRD), and extended X-ray absorption fine structure (EXAFS) measurements. The activity of these catalysts was measured at 643 K and 3.1 MPa in a three-phase, packed-bed reactor for hydrodesulfurization (HDS), hydrodenitrogenation (HDN), and hydrodeoxygenation (HDO) using a model liquid feed containing 3000 ppm S as dibenzothiophene, 2000 ppm N as quinoline, and 500 ppm O as benzofuran. An optimum Ni_2P loading for HDS, HDN, and HDO activity was found around 18 wt% which gave an HDS conversion of 99%, an HDN conversion of 91%, and an HDO conversion of 80% at a WHSV of 2.1 h^{-1}. These were much higher than those of a commercial $Ni–Mo–S/Al_2O_3$ catalyst which gave an HDS conversion of 76%, and an HDN conversion of 38% based on equal sites (70 μmol) loaded in the reactor. The sites were counted by CO chemisorption for the phosphide and by low-temperature O_2 chemisorption for the sulfide. XRD and EXAFS results confirmed that a Ni_2P phase was formed on the support. The crystallite size increased slightly from 7.7 to 9.8 nm when the loading was increased, and there was evidence from CO chemisorption that some crystallite agglomeration occurred in the higher loading samples. It was found that the HDS performance did not change appreciably with Ni_2P loading, but that the HDN activity and stability went through a maximum at intermediate loading. It was concluded that the HDS reaction is structure-insensitive, while the HDN reaction depends on the local arrangement of surface Ni, P, and S atoms, and is structure-sensitive. XRD and EXAFS analysis indicated that the active catalyst formed a surface phosphosulfide phase on top of a Ni_2P core in the course of hydrotreating.

Keywords: Structure sensitivity; Nickel phosphide; XRD; EXAFS; HDN; HDS

1. Introduction

Transition metal phosphides have recently been reported as members of a new class of high-activity catalysts [1–5] for hydrodesulfurization (HDS) and hydrodenitrogenation (HDN) of petroleum feedstocks. These materials are compounds between phosphorus and transition metals and combine physical properties such as hardness and strength typical of ceramics, and electronic properties like conductivity characteristic of metals [6]. Initial studies with the iron group phosphides, Fe_2P, CoP, Co_2P, and Ni_2P [7–9] indicated that their activity was low to moderate, with Ni_2P supported on silica having the highest activity. However, it was recently found in a study of the effect of initial Ni/P ratio on the structure and hydroprocessing behavior of Ni_2P/SiO_2 [10] that increasing the initial phosphorus content from the stoichiometric Ni/P ratio of 1/0.5 to a four-fold excess of 1/2 substantially enhanced conversion in both HDS and HDN to unprecedented levels. Thus, for the reaction of dibenzothiophene an HDS conversion of 100% was obtained, and for the reaction of quinoline an HDN conversion of 81% was observed [10]. Even in the conversion of a real feed, this material showed better activity, selectivity, and stability than a commercial $Co–Mo–S/Al_2O_3$ [11].

It was found in our previous study [10] that the Ni/P ratio had a minimal effect on the HDS activity of the samples, but a considerable one in the HDN activity. It was deduced that on Ni_2P the HDS reaction was structure insensitive but the HDN reaction was structure sensitive. The initial motivation of the present study was to further examine the structure sensitivity of the reactions by the classical technique of variation of particle size through the preparation of samples with different loadings. However, it was found that for the phosphides particle size could not be

* Corresponding author.
E-mail address: oyama@vt.edu (S.T. Oyama).

0021-9517/$ – see front matter
doi:10.1016/S0021-9517(03)00017-4

changed broadly as with metals due to the severe preparation conditions. Nevertheless, the samples of different loading showed differences in composition which were accompanied by small changes in HDS activity but substantial variations in HDN activity, consistent with the original suggestion that HDS was structure-insensitive and HDN was structure-sensitive.

The conclusions of this study are based on careful preparation and characterization of samples. The preparation of the samples was carried out as before by the temperature-programmed reduction (TPR) of supported phosphate precursors containing excess initial phosphorus (Ni/P = 1/2), but with different concentrations of the active phase. X-ray diffraction (XRD) analysis after preparation showed that the phase present was Ni_2P, and this was confirmed by elemental analysis which indicated a phosphorus content slightly in excess of stoichiometric (Ni/P = 1/0.5) for samples after reaction. Gravimetric measurements and elemental analysis in this study indicated that the excess phosphorus was not vaporized during the calcination step of preparation of the phosphate precursors, but that the excess phosphorus was lost mainly during the reduction step. Mass spectrometry showed the production of PH_3 during the TPR process. Extended X-ray absorption fine structure (EXAFS) analysis on samples protected from the atmosphere confirmed the results obtained by XRD that showed that the predominant phase in the freshly prepared samples was Ni_2P.

It was also found in this study that the catalysts underwent several changes during the course of the hydroprocessing reactions. First, an increase in the XRD line intensities indicated that the Ni_2P particles underwent crystallization. Second, elemental analysis showed that the catalysts took up small amounts of sulfur. Finally, EXAFS analysis indicated the formation of Ni–S bonds. The overall results are consistent with the formation of a crystalline core of Ni_2P covered with a surface phosphosulfide phase. Differences in the arrangement of the Ni, P, and S atoms on the surface gave rise to the observed structure sensitivity in the HDN reaction. Under the conditions of the earlier study [10] the best catalyst in the present work had an HDS conversion of 98% and an HDN conversion of 91%. This is a substantial improvement over the previous results, and the catalyst is one of the most active on record on the basis of active sites loaded in the reactor.

2. Experimental

2.1. Materials

The support used in this study was a fumed silica (Cabosil, L-90). The chemicals used in the synthesis of the catalysts were $Ni(NO_3)_2 \cdot 6H_2O$ (Aesar, 99%) and $(NH_4)_2HPO_4$ (Aldrich, 99%). The chemicals utilized in the reactivity study were dibenzothiophene (Aldrich, 99.5%), quinoline (Aldrich, 99.9%), benzofuran (Aldrich, 99.9%), tetralin (Aldrich, 99.5%) and tetradecane (Jansen Chimica, 99%). The gases employed were He (Airco, Grade 5, 99.99%), CO (Linde Research Grade, 99.97%), 0.5% O_2/He (Airco, UHP Grade, 99.99%), H_2 (Airco, Grade 5, 99.99%), N_2 (Airco, 99.99%), and 30% N_2/He (Airco, UHP Grade, 99.99%).

2.2. Synthesis and characterization of catalysts

Detailed preparation procedures have been described elsewhere [10] and only a synopsis needs to be presented here. Briefly, the synthesis of the catalysts involved two stages. First, intermediate precursors of nickel phosphate on silica were obtained by incipient wetness impregnation of aqueous nickel phosphate solutions prepared from nickel nitrate and ammonium phosphate, followed by drying and calcination at 773 K. Second, the precursor materials were reduced to phosphides in H_2 flow by the method of temperature-programmed reduction to 850 K, and were subsequently passivated in 0.5% O_2/He at room temperature for 2 h. The amounts of the reagents used and the weight of the precursors collected after calcination are listed in Table 1. In the previous study of these materials [10], the metal loading was kept constant at a level corresponding to the 12.2 wt% Ni_2P with an initial Ni/P ratio of 1/2. For this reason, this loading level will be referred to in this paper as a loading level of 1.0. Relative to this level, other loading levels are designated as 0.5, 1.5, and 2.0 (Table 1).

Irreversible CO uptake measurements were used to titrate the surface metal atoms and to provide an estimate of the active sites on the catalysts. They were obtained by pulsing calibrated volumes of CO into a He carrier and measuring the decrease in the peak size caused by adsorption. Uptakes were obtained after passivation and rereduction of samples, and are denoted as ex situ uptakes. BET surface area measurements were carried out right after the CO uptake determinations, also using a flow technique [10]. The areas were calculated from the one-point BET equation, which is applicable for the nonmicroporous samples used here. X-ray diffraction patterns of both fresh and spent samples were determined with a Scintag XDS-2000 powder diffractometer operated at 45 kV and 40 mA, using Cu-K_α monochromatized radiation ($\lambda = 0.154178$ nm). Crystallite sizes of the spent catalysts were determined from the line broadening of the two most intense peaks at $2\theta = 40.8^\circ$ ($hkl = 111$) and at $2\theta = 44.6^\circ$ ($hkl = 201$). Use was made of the Scherrer equation, $D_c = K\lambda/\beta\cos(\theta)$, where K is a constant taken as 0.9, λ is the wavelength of the X-ray radiation, β is the width of the peak at half-maximum corrected for instrumental broadening (0.1°), and 2θ is the Bragg angle [12].

Elemental analysis of the samples was carried out using an inductively coupled plasma atomic emission spectrometer (ICP-AES, Spectro Analytical Instruments, Model Spectroflame FTMO A85D). For the measurements the samples were subjected to aqua regia digestion in a microwave oven (EthosPlus, Milestone).

In order to determine whether the structure of the catalysts changed with loading and with reaction, the catalysts were examined using EXAFS analysis. Nickel K-edge EXAFS spectra were obtained for both fresh and spent samples. Both the freshly prepared samples and the spent samples were transferred to glass cells with Kapton windows and were sealed by glassblowing without exposure to the atmosphere. The spent samples were removed from the reactors, washed with hexane, dried, and treated in He flow at 723 K before the transfer. For the EXAFS analysis comparisons were made with several reference materials, Ni_2P (Cerac, 99.5%), NiO (Cerac, 99%), NiS (Cerac, 99.9%), $NiCO_3[Ni(OH)_2]\cdot 4H_2O$ (Aldrich). The measurements were made in a transmission mode at the BL12C beamline in the Photon Factory, High Energy Laboratory in Tsukuba, Japan, and at the X18B beamline in Brookhaven National Laboratory. Both were operated at close to 2.5 GeV with a 300–400 mA ring current. The monochromator in Tsukuba was equipped with a channel cut Si (311) crystal and gave an energy resolution of about 1 eV, while that in Brookhaven used a Si (111) crystal and resulted in an energy resolution of 2 eV.

The obtained EXAFS data were analyzed by Winxafs 97 and UWWAFS 3.0 software. FEFF simulations to obtain phase shifts and amplitude functions of Ni_2P and $Ni_{12}P_5$ were done with FEFF 8.0 code [13]. The FEFF input file for the simulation consisted of the cluster size (0.6 nm), atomic positions, and type of atoms obtained from crystallographic data from the literature [14,15].

2.3. Reactivity studies

Hydrotreating activities of the samples were measured in a three-phase, packed-bed reactor operated at 3.1 MPa and 643 K for hydrodenitrogenation, hydrodesulfurization, hydrodeoxygenation (HDO), and hydrogenation (HYD) of a model feedstock containing 2000 ppm nitrogen (quinoline), 3000 ppm sulfur (dibenzothiophene), 500 ppm oxygen (benzofuran), 20 wt% aromatics (tetralin), and balance aliphatics (tetradecane). The HDS conversion refers to the transformation of dibenzothiophene to biphenyl, the HDN conversion to the reaction of quinoline to denitrogenated products, the HYD conversion to the reaction of quinoline to N-containing hydrogenated products (1,2,3,4-tetrahydroquinoline, 5,6,7,8-tetrahydroquinoline, orthopropylaniline), and the HDO conversion to the reaction of benzofuran to ethylbenzene. The schematic of the testing system was shown elsewhere [16]. Briefly, the testing unit consisted of three parallel reactors immersed in a fluidized sand bath (Techne, Model SBL-2) whose temperature was controlled by a temperature controller (Omega, Model 6015 K). The reactors were 19/16 mm o.d./i.d. 316 SS tubes with central thermocouples monitoring the temperature of the catalyst beds. The catalysts were in the form of pellets (16/20 mesh) and were supported between quartz wool plugs in 13 mm i.d. 316 stainless-steel baskets. The hydrogen flow rate was set to 100 μmol s^{-1} (150 $cm^3\,min^{-1}$, NTP) with mass flow controllers (Brooks, Model 5850E), and the feed liquid flow rate (5 $cm^3\,h^{-1}$) was metered from burettes by high-pressure liquid pumps (LDC Analytical, Model NCI 11D5). Quantities of catalysts loaded in the reactors corresponded to the same amount of ex situ CO uptake (70 μmol). The passivated catalysts were rereduced under H_2 at 723 K for 2 h before the feed liquid was introduced into the reactors. Hydrotreating samples were collected every 2 or 3 h in sealed septum vials and were analyzed by a gas chromatograph (Hewlett Packard, 5890A) equipped with a 0.32 mm i.d. × 50 m fused silica capillary column (CPSIL-5CB, Chrompack, Inc.) and a flame ionization detector.

3. Results and discussion

The supported phosphides were prepared by the temperature-programmed reduction of supported phosphate precursors. The amounts of reagents used and the resulting loadings are summarized in Table 1. The quantity of phosphorus used in the syntheses was four times that required for formation of Ni_2P. The excess phosphorus was used because previous work had shown that an amount of phosphorus above stoichiometric proportions was necessary in order to obtain an active catalyst [10]. Assuming that after calcination the product was a mixture of nickel phosphate (Ni_2PO_4) and a surface phosphorus oxide (taken as P_2O_5), the weight of product expected is reported in the last column of Table 1. The calculated weight is in good agreement with the measured weight, indicating that the proposed phosphate products were likely to be formed. The agreement also indicated that there was no volatilization of phosphorus in the calcination stage.

Table 1
Quantities used in the preparation of the samples

Loading	Materials used			Phosphide loading	Weight after	Weight
level	Silica (g)	Nickel nitrate (mol)	$(NH_4)_2HPO_4$ (mol)	(wt% MP_x)	calcination (g)	calculated[a] (g)
0.5	20	0.0115	0.0231	6.5	22.5	22.5
1.0	20	0.0231	0.0462	12.2	25.0	24.9
1.5	20	0.0387	0.0693	18.1	27.7	27.7
2.0	20	0.0462	0.0924	21.8	30.4	29.8

[a] $Ni_2(PO_4) + 3/2P_2O_5$.

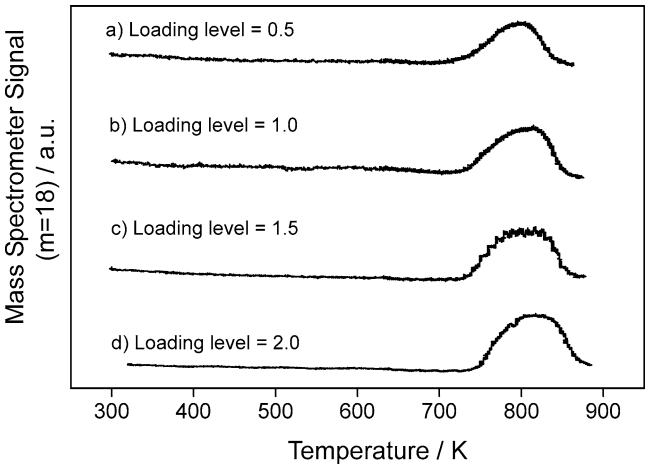

Fig. 1. Mass 18 signal from temperature-programmed reduction of the samples at $\beta = 1\ \mathrm{K\,min^{-1}}$ ($0.01667\ \mathrm{K\,s^{-1}}$).

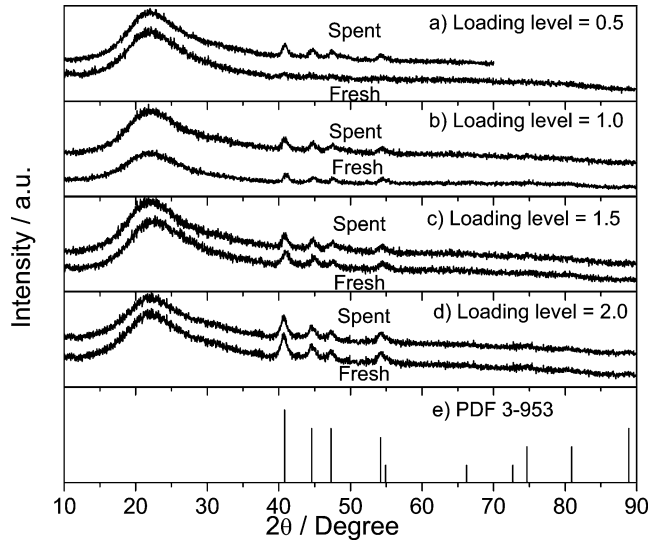

Fig. 2. X-ray diffraction patterns of the fresh and spent samples and comparison to Ni_2P (PDF 3-953).

Fig. 1 shows the water evolution during the temperature-programmed reduction stage of the synthesis. Mass 34 (PH_3) followed the same trend as the water signal and is not displayed here. It is clearly seen that the reduction reactions for all the samples essentially occurred in the same temperature range, except that a slightly higher temperature was required for the higher loading samples (Figs. 1c–1d). This is understandable since larger phosphate particles are probably present on the higher loading catalysts, which present larger pathways for diffusion in the solid-state reduction process.

X-ray diffraction patterns of the fresh and spent samples are presented in Fig. 2. The patterns all show a broad feature at $2\theta \sim 22°$ due to the amorphous silica support. At higher angles, peaks due to Ni_2P are visible at all loadings. The phase corresponds to hexagonal Ni_2P [17] which adopts the Fe_2P structure with a space group of $P_{\bar{6}2m}$. The pattern is presented in the powder diffraction file PDF 3-953 (Fig. 2e) [18].

X-ray diffraction patterns for the spent samples (Fig. 2) show that there were no changes in the peak positions after reaction, demonstrating that the Ni_2P was stable under the hydrotreating conditions. However, the intensity of the XRD peaks for the spent samples increased, which indicates that the samples became more crystallized. The crystallization was likely a consequence of the prolonged exposure (> 100 h) of the samples to the hydrotreating temperature of 643 K.

The elemental analysis of the samples is given in Table 2. All of the samples were prepared with an initial Ni/P ratio of 1/2 with a varying loading amount as reported in Table 1. Results are shown for freshly reduced samples (fresh) and for used samples (spent) after reaction for either 100 or 300 h. In the case of the sample with loading level of 1.0, elemental analysis of the precursor phosphate material (calcined) is also reported.

In all cases the freshly prepared samples were found to have phosphorus contents that were smaller than the initial

Table 2
Elemental analysis results (loading level = 1.0 represents 12.2 wt% Ni_2P)

Loading level	Sample	Composition (wt%)			Ni/P molar ratio	Ni/S molar ratio
		Ni	P	S		
0.5	Fresh	2.80	1.32	–	1/0.89	–
	Spent[a]	2.76	0.88	0.0518	1/0.60	1/0.019
1.0	Calcined	5.76	6.09	–	1/1.99	–
	Fresh	5.73	2.52	–	1/0.83	–
	Spent[a,b]	5.63	1.71	0.162	1/0.57	1/0.029
	Spent[c]	5.45	1.65	0.292	1/0.57	1/0.054
1.5	Fresh	8.51	3.22	–	1/0.73	–
	Spent[a]	8.46	2.55	0.101	1/0.58	1/0.012
2.0	Fresh	10.70	4.00	–	1/0.71	–
	Spent[c]	9.9	3.24	0.301	1/0.61	1/0.030

[a] Reaction time: 100 h.
[b] Initial Ni/P ratio = 1/1.8.
[c] Reaction time: 300 h.

value, with Ni/P ratios ranging from 1/0.71 to 1/0.89. For the sample with loading level of 1.0, the Ni/P ratio for the calcined sample was 1/1.99, very close to the initial amount of 1/2. These findings indicate that the phosphorus loss occurred during the reduction step of the preparation, not the calcination stage. This is consistent with the weight measurements of the calcined samples (Table 1). It is also in agreement with the results of the TPR analysis which indicated the production of PH_3 during the reduction, as also observed in a previous study [10].

Elemental analysis also showed that there was a further reduction in phosphorus content in the course of reaction, with the Ni/P ratios for the spent samples ranging from 1/0.57 to 1/0.60. These values are close to the ratio of 1/0.50, corresponding to the Ni_2P stoichiometry, and is consistent with the formation of that phase as shown by the XRD patterns. The slight remainder of the phosphorus

probably resides on the support as unreduced phosphate. In the case of the sample with loading level of 1.0, which was tested in two runs of different duration (100 and 300 h), it was observed that prolonged reaction did not change the Ni/P ratio. This indicates that after a period of reaction the catalyst lines out and becomes stable. The decrease in P content from the initial value before reaction for that sample would give rise to a P content of 0.6 ppm in the effluent stream, which is below the sensitivity for analysis in the gas chromatograph. Thus, no extraneous peaks were observed in the reaction product analysis.

Sulfur content determinations by elemental analysis of the spent samples were also carried out and are reported as Ni/S atomic ratios (Table 2). In all cases there was some sulfur taken up by the catalysts. The samples that had undergone reaction for longer times (300 vs 100 h) had larger amounts of sulfur. For the samples after 100 h, the Ni/S ratio ranged from 1/0.012 to 1/0.029, and for the samples after 300 h, the Ni/S ratio ranged from 1/0.030 to 1/0.054. These amounts of sulfur were moderate; on the average the molar sulfur level was about 5% of the phosphorus content. The location of the sulfur cannot be totally ascertained. As will be seen from the EXAFS analysis, the sulfur likely interacts with the surface of the phosphide crystallites to form a phosphosulfide phase. However, some of the sulfur may reside on the support. The phosphosulfide is formed on the surface, as the XRD results indicate that the bulk of the crystallites remain Ni_2P. Also the surface is not a pure sulfide, as the reactivity of nickel sulfide is known to be poor [19].

The surface properties of the fresh catalysts are also shown in Table 3. X-ray line-broadening analysis of the spent samples indicated a weak trend toward larger crystallite sizes with increasing sample loading. The crystallite sizes are listed in the last column of Table 3 and are seen to increase from 7.7 to 9.8 nm. The small effect of loading on crystallite size is probably due to the high temperature required for preparation. The synthesis involves the reduction of a phosphate phase, which is a relatively difficult transformation because of the need to break stable P–O bonds. The severe conditions cause sintering of the phosphide crystallites. As will be seen, it was also found that a low loading sample was particularly difficult to prepare with the right stoichiometry. This may represent a limitation for the preparation of samples consisting of compounds from two elements like nickel phosphide. However, it was found in this study that catalysts of intermediate loading had high activity.

Table 3
Characterization results of samples

Loading level[a]	Samples	BET surface area (S_g) ($m^2\,g^{-1}$)	CO uptake ($\mu mol\,g^{-1}$)	Metal site density (L) ($\mu mol\,g^{-1}$)	D_c (nm)
0.5	Fresh	74	23	85	–
	Spent	88	7	85	7.7
1.0	Fresh	97	28	170	–
	Spent	89	24	170	8.7
1.5	Fresh	102	40	254	–
	Spent	98	45	254	9.2
2.0	Fresh	72	37	339	–
	Spent	83	27	339	9.8

[a] The loading level of 1.0 corresponds to 12.2 wt% Ni_2P/SiO_2.

The BET specific surface areas (S_g) and CO chemisorption uptakes of the samples are listed in columns 3 and 4 of the table, respectively. The S_g values of the samples were of the order of that of the silica support ($90\ m^2\,g^{-1}$) with deviations due to experimental error with the flow technique. The CO chemisorption uptake for the fresh samples increased with increase of the Ni_2P loading, reaching a maximum value of 40 $\mu mol\,g^{-1}$, and then decreased. The results indicate that there is probably crystallite agglomeration on the higher loading samples, resulting in a slightly poorer dispersion of Ni_2P, and hence giving lower CO chemisorption. Metal site concentrations were obtained from the crystallite size (D_c) and the known density of metal atoms ($\bar{n} = 1.01 \times 10^{15}$ atoms cm^{-2}) from the crystal structure [7]. The metal site concentration was calculated from the equation, $(L) = S\bar{n}f$, where f is the fractional weight loading of the sample (Table 1), and $\bar{n}$ is the average surface metal atom density, S is the theoretical surface area obtained from the equation, $S = 6/\rho D_c$. The results are listed in the fifth column of Table 3, and are seen to increase with increasing loading amount. The number of metal sites is much higher than the sites titrated by CO uptake. This could be due in part to the agglomeration of the crystallites noted above. As can be seen, there is a greater difference in the two values at higher loadings, consistent with this interpretation. However, the differences are too large to be explained by just agglomeration, and it is likely that CO chemisorption sites are blocked by surface phosphorus. The increase of the number of chemisorption sites should be one of the objectives of future research.

Figs. 3 and 4 present the time course of HDS and HDN activities for the various catalysts, reported as the dibenzothiophene and quinoline conversions, respectively. The HDS activity was uniformly high for all the samples with an HDS conversion at 97–99% and was stable (Fig. 3). This indicates that the HDS reaction is structure insensitive over these catalysts. In contrast, the HDN activity varied considerably with Ni_2P loading and for some samples showed deactivation (Fig. 4). The samples with intermediate loading levels of 1.0 and 1.5 followed similar time courses, with the sample of loading level 1.5 showing good stability. The final HDN conversions for these samples were 81 and 91%, respectively. The sample with the lowest and highest loading levels deactivated quickly and reached a low HDN activity below 40%. As will be seen, this was due to incomplete formation of phosphide in the sample with the lowest loading level, and because of site poisoning in the sample with highest loading level. A summary of all the results is presented

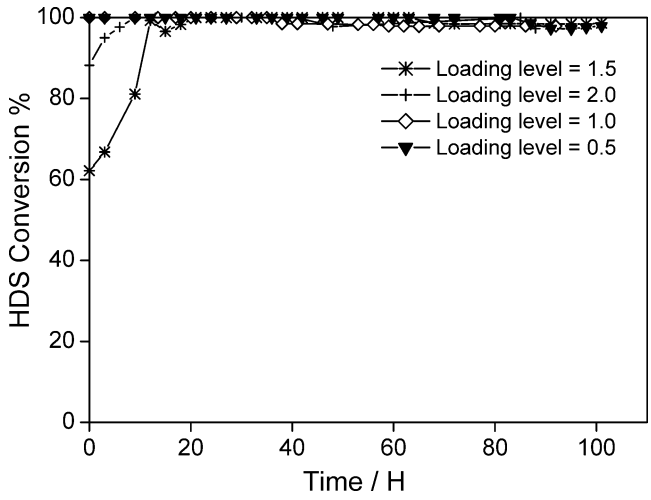

Fig. 3. Hydrodesulfurization performance of supported catalysts.

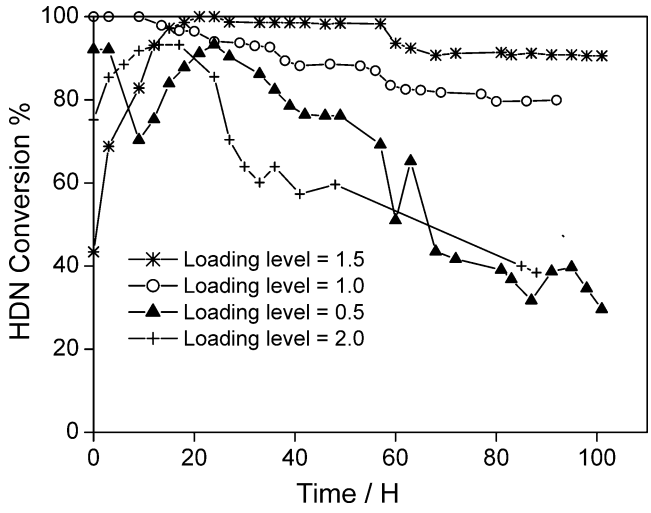

Fig. 4. Hydrodenitrogenation performance of supported catalysts.

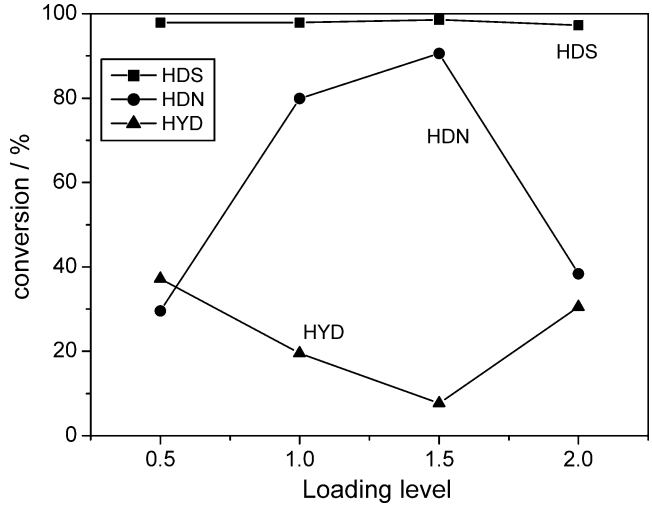

Fig. 5. Comparison of hydroprocessing activities.

in Fig. 5, which shows the effect of loading on the activity of all the catalysts. The best performance was obtained at a loading level of 1.5 with an HDS conversion of 99% and an HDN conversion of 91% at a WHSV of 2.1 h^{-1}. Hydrogenation of quinoline to N-containing compounds (HYD) is low for this sample, a desirable characteristic for the catalyst. The activity difference in HDN is likely due to the structure sensitivity of the reaction. This will be discussed in more detail later.

Compared to a commercial Ni–Mo–S/Al_2O_3 catalyst, which gave an HDS conversion of 76% and an HDN conversion of 38% [10], the Ni_2P/SiO_2 with loading level 1.5 was substantially more active. The comparison here is based on 70 μmol of sites loaded in the reactor, the sites counted by CO chemisorption for the phosphides and O_2 chemisorption for the sulfide. Thus, the comparison shows that the intrinsic activity of the phosphide is very high.

A full report of the activity and selectivity of the catalysts is presented in Table 4. The table is organized with the reactants shown in the first column, the reaction type in the second column, and a set of conversions and selectivities for the samples with different loading levels in subsequent columns. The selectivities add up to 100% for each reaction type. The reaction of dibenzothiophene occurs with very high conversion (97–99%) on all catalysts and gives total selectivity to biphenyl. On sulfides the lack of a hydrogenated intermediate like phenylcyclohexane has been cited as an indication that the reaction occurs by direct sulfur removal from dibenzothiophene [20,21]. This is likely for the nickel phosphide catalyst, and would be consistent with the observed structure-insensitive nature of the reaction. The hydrogenation route to desulfurization requires more active sites.

Quinoline can react to form HDN and HYD products, and the two conversions are indicated. Because these are parallel reactions, a high conversion for HDN is accompanied by a low conversion in HYD. The conversion of quinoline in HDN is low at the smallest and largest loading level but is high (81–91%) at intermediate loading levels. The products can be classified as hydrogenated molecules (5,6,7,8-tetrahydroquinoline, orthopropylaniline, 1,2,3,4-tetrahydroquinoline) and denitrogenated species (propylcyclohexane, propylbenzene). At high HDN conversions propylcyclohexane is favored because of the likely need to hydrogenate the two aromatic rings prior to nitrogen removal. The reason for the high conversion is likely to be due to an optimal arrangement of catalytic functions on the catalyst surface. This will be discussed further after the EXAFS results are presented.

Benzofuran is completely deoxygenated to ethylbenzene on all catalysts, notably with 80% conversion for the catalyst with intermediate loading level of 1.5. HDO is a facile reaction compared to HDS and HDN, and probably does not interfere with the S- and N-removal reactions. For thermodynamic reasons, because of the high temperature of reaction (643 K) dehydrogenation is favored over hydrogenation. Thus, tetralin is mostly dehydrogenated to

Table 4
Product distribution in hydroprocessing

Reactants	Reaction	Conversion (%) of loading level				Products	Selectivity (%) of loading level			
		0.5	1.0	1.5	2.0		0.5	1.0	1.5	2.0
Dibenzo thiophene	HDS	98	98	99	97	Biphenyl	100	100	100	100
Quinoline	HDN	30	81	91	38	Propylcyclo-hexane	8.9	50	53	4.7
						Propylbenzene	17	28	38	22
	HYD	37	19	7.7	31	5,6,7,8-Tetrahydro-quinoline	27	3.9	2.0	22
						Orthopropyl-aniline	37	15	4.8	33
						1,2,3,4-Tetrahydro-quinoline	11	3.7	1.8	18
Benzofuran	HDO	37	46	80	50	Ethylbenzene	100	100	100	100
Tetralin	De-HYD	44	23	36	55	Naphthalene	98.8	94.9	96.6	99.0
	HYD	0.5	1.2	1.2	0.6	*trans*-Decalin	0.5	2.7	2.2	0.3
						cis-Decalin	0.7	2.4	1.2	0.7

Catalyst loading based on 70 μmol CO uptake.

naphthalene. Small amounts of *cis*- and *trans*-decalin are also formed, in comformity with equilibrium.

The CO uptakes for the spent samples are listed in Table 3. The values decreased for all samples except for the active sample with loading ratio of 1.5. The decrease was particularly pronounced for the catalysts with the lowest and highest loadings. This loss of active centers may be an important reason for the deactivation of the catalysts (Fig. 4).

Fig. 6 presents the HDN and HDS turnover rates (TORs) based on CO uptakes before reaction and the CO chemisorption values themselves for both the fresh and spent samples as a function of loading level. The CO uptakes of the fresh samples increase with loading, but not as much as expected from the crystallite size and concentration. At the highest loading level, they decrease slightly. As discussed previously this indicates some crystallite agglomeration on the higher loading samples, especially in the sample with the loading level of 2.0. The hydroprocessing TORs results indicate that HDS reactions are not affected by the surface properties of the catalysts, while the HDN reactions are very sensitive to

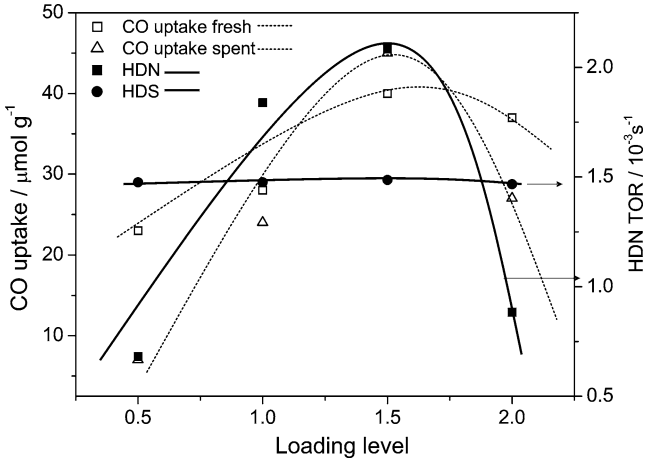

Fig. 6. Curves of HDN and HDS turnover rates and CO uptakes.

the structure or composition of the catalyst surface. In a previous study of the mechanism of HDN on MoP and WP [4] it was established that denitrogenation occurred through an E2 elimination involving dual acid and nucleophilic centers on the surfaces. The need for such surface centers also in the case of Ni_2P would make the reaction sensitive to the exact arrangement of Ni, P, and possibly S atoms on the surface, and would explain the strong effect of loading on HDN. The HDN turnover rate tracks well with the CO uptake of the spent catalysts. Since CO adsorbs on only one metal center, this would indicate that the catalyst site contains only one coordinatively unsaturated Ni atom, and it is the arrangement of surrounding atoms that causes the structure sensitivity in HDN.

Both the fresh and the spent samples were analyzed by EXAFS spectroscopy. The Ni K-edge EXAFS spectra for the fresh samples with loading levels of 0.5, 1.0, 1.5, and 2.0 were compared with those of bulk Ni_2P, NiO, $Ni(OH)_2$, and Ni metal (Fig. 7). The Fourier transforms (FT) for the supported Ni_2P samples are characterized by two prominent peaks in the bonding region (> 0.13 nm) (Fig. 7a–7d). For the higher loading levels of 1.0 and above (Fig. 7b–7d), the position of the peaks correspond to the Ni–P and Ni–Ni distances in bulk Ni_2P (Fig. 7e). The relative intensity of the peaks also are close to those of bulk Ni_2P, although the sample with the highest loading level 2.0 shows enhanced intensity (Fig. 7d) at the Ni–Ni peak. This would indicate some propensity for overreduction when the loading of the active phase is high.

For the lowest loading level of 0.5 (Fig. 7a), the FT peaks shifted to lower distances from those of Ni_2P. The Ni–Ni distance was displaced toward that of metallic Ni (Fig. 7h), whereas the shorter distance peak was displaced toward that of a Ni–O bond in NiO (Fig. 7f) or $Ni(OH)_2$ (Fig. 7g). It appears that incomplete phosphidation occurred in this sample, and that as the material was reduced some Ni–Ni and Ni–O bonding contributions were formed. This is consistent with

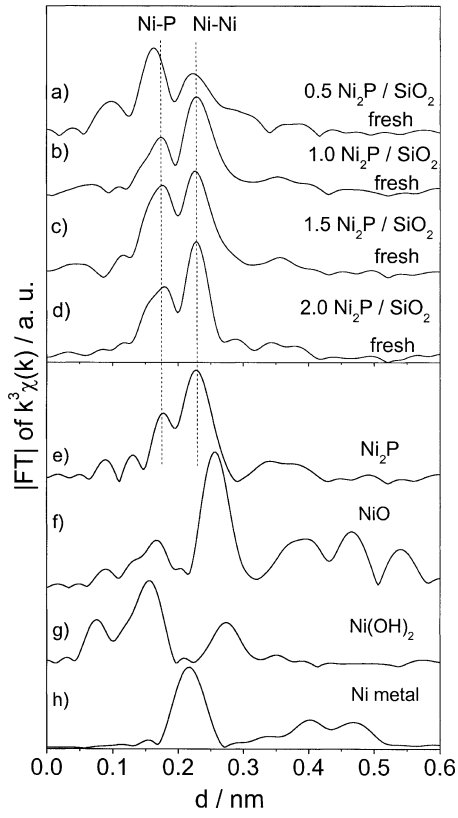

Fig. 7. Comparison of nickel K-edge EXAFS for the fresh samples with loading ratio of 0.5, 1.0, 1.5, 2.0, and Ni_2P, NiO, $Ni(OH)_2$, and nickel metal.

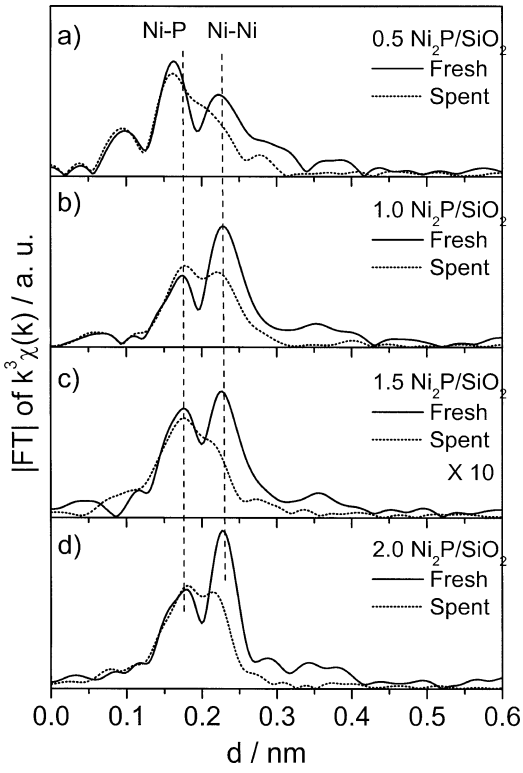

Fig. 8. Nickel K-edge EXAFS of the fresh and spent samples with different loading (12.2 wt% here was used as loading level 1.0). (a) Loading level = 0.5; (b) loading level = 1.0; (c) loading level = 1.5; (d) loading level = 2.0.

the XRD patterns, which gave very weak signals for Ni_2P for this sample.

Ni K-edge EXAFS results for both fresh and spent samples are compared in Fig. 8. The features of the fresh samples (solid lines) and the spent samples (dashed lines) were different, especially in the Ni–Ni peak region. The intensity of the Ni–Ni peak decreased after hydrotreating for all the samples, and it is likely that some other nickel compounds were formed as a consequence of the reaction.

The EXAFS results of the spent samples (Fig. 9a–9d) were compared with some reference compounds (Fig. 9e–9i) to identify the newly formed phase. The diminution in the intensity of the Ni–Ni peak in Ni_2P for the samples (Fig. 9a–9d) seemed to be accompanied with a shift to lower distance. The Ni–P peak itself remained strong, though slightly diminished in distance. The result could be due to the formation of some phosphorous deficient Ni phase, but also could be due to development of intensity in the Ni–S distance region. Even though no distinct Ni–S peak is seen, a feature in that region would give rise to the broad signal actually observed. Fig. 9c–9d shows just such a fit to three Lorentzian line shapes for the higher loading samples. The middle peak of each triad fits the position of the Ni–S distance in the sulfide reference compounds (Fig. 9h,9i).

In a previous study of Ni_2P/SiO_2 of different Ni/P ratios an XRD peak that could be due to $Ni_{12}P_5$ was observed for a spent sample with Ni/P = 1/1 [10]. In order to check the possibility of formation of a phosphorus-deficient phase, calculation of the EXAFS of $Ni_{12}P_5$ was carried out. First, the applicability of FEFF calculations was checked with Ni_2P. The FEFF simulation of Ni_2P produced a similar EXAFS oscillation compared to the experimental result of Ni_2P (Fig. 10a). In the higher k-region (>80 nm^{-1}), the amplitude of the calculated oscillation was stronger than that of the experimental spectrum, due to thermal broadening in the latter spectrum. However, the periods of both EXAFS oscillations were quite similar. A comparison of the Fourier transforms of bulk Ni_2P and the FEFF simulation also showed good agreement (Fig. 10b). The first and second nearest neighbors corresponding to Ni–P and Ni–Ni bonds in bulk Ni_2P were identical to those obtained in the FEFF simulation (Table 5). Moreover, the third and fourth shells of the Fourier transforms also showed good agreement. This indicates that the FEFF simulation is able to account for the essential elements of the bulk Ni_2P structure.

The synthesis of $Ni_{12}P_5$ as a reference material was attempted by the ampoule technique (heating stoichiometric amounts of Ni metal and phosphorous powder in a sealed quartz ampoule at 1073 K for 100 h), but was unsuccessful. Therefore, resort was made to a FEFF simulation. The results are shown in Figs. 10c and 10d. The simulation clearly shows that slightly reduced Ni–Ni and Ni–P distances compared to Ni_2P are to be expected for $Ni_{12}P_5$. Clearly the shape of the simulated spectrum does not match the spectra

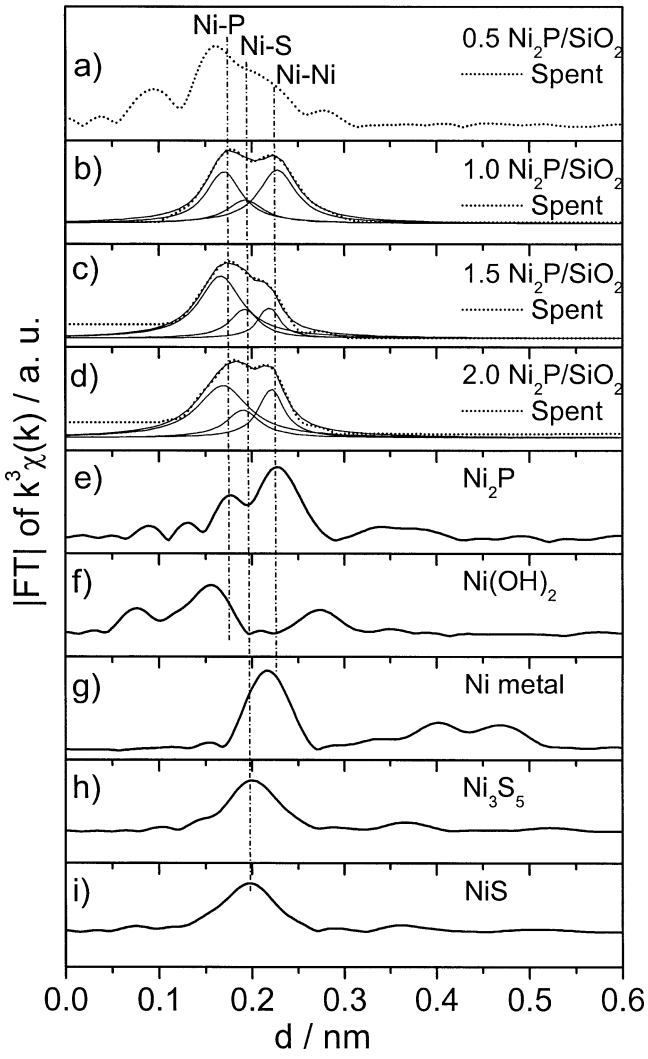

Fig. 9. Comparison of nickel K-edge EXAFS for the spent samples with loading levels 2.0, 1.5, 1.0, 0.5, and Ni_2P, $Ni(OH)_2$, nickel metal, Ni_3S_5, and NiS.

of the spent samples. What the EXAFS data strongly suggest though is that in the catalysts Ni–Ni bonds are disrupted in favor of the formation of some Ni–S linkages. Thus, the active catalyst in these materials is probably a Ni–P–S surface phase on the outer region of a Ni_2P crystallite core. The presence of three elements in different arrangements causes the activity of the catalysts in the HDN and HDS reactions to be affected differently (Table 6).

Based on the influence of surface properties on the activity, Boudart categorized reactions as "structure sensitive" and "structure insensitive" [22,23]. This proves to be a valuable concept for these new catalysts. The structure sensitivity arises in this case not from a particle size effect, but from structural differences induced by composition in the active surface phase which contains Ni, P, and S. The results shown in this work are consistent with the HDS reaction of dibenzothiophene being structure insensitive, and the HDN reaction of quinoline being structure sensitive.

Table 5
Summary of structural parameters used in FEFF simulation

Ni_2P			$Ni_{12}P_5$		
Bonding	Coordination number	Distance (nm)	Bonding	Coordination number	Distance (nm)
Ni–P	**2**[a]	**0.22090**[a]	Ni–P	**1**[a]	**0.22294**[a]
	2[a]	**0.22662**[a]		**1**[a]	**0.22504**[a]
	2	0.37042		1	0.24245
	4	0.40393		1	0.24625
Ni–Ni	2	0.26050	Ni–Ni	1	0.25249
	2	0.26131		1	0.25451
	4[a]	**0.26783**[a]		1	0.25472
	2	0.33820		1	0.25720
	4	0.38260		1	0.25955
	4	0.42739		**2**[a]	**0.26347**[a]
	4	0.43339		1	0.27031
				2	0.36280
				2	0.36492
				2	0.36632
				4	0.48636

[a] Major contributions in the simulation.

4. Conclusions

This work was carried out to complement an earlier study [10] of the effect of Ni/P ratio on the structure and hydroprocessing behavior of Ni_2P/SiO_2, which had shown that maximum activity was obtained on samples prepared with an initial Ni/P ratio of 1/2. In this study the effect of loading (6–22 wt%) on Ni_2P/SiO_2 with the same initial Ni/P ratio of 1/2 was investigated to examine the structure sensitivity of the HDS and HDN reactions, and similar conclusions were reached. Although here it was found that loading did not have a major effect on the crystallite sizes of the supported nickel phosphide phase, which varied only between 7.7 to 9.8 nm, differences in the reactivities of the catalysts indicated that the HDN reaction of quinoline was structure sensitive, while the HDS reaction of dibenzothiophene was structure insensitive. The reactivity differences were ascribed to variations in surface composition with loading. This was the same conclusion reached in the earlier study. XRD, EXAFS, and elemental analysis on all the fresh samples showed the formation of a Ni_2P phase. Analysis of the spent samples showed that they underwent a surface phase change which resulted in the formation of a phosphosulfide layer on top of the Ni_2P phase. In the low loading sample which had poor activity incomplete formation of the Ni_2P phase was found. In the high loading sample which also had low activity, formation of Ni–Ni bonds was observed, suggestive of overreduction. The best catalyst of intermediate loading had the best balance of Ni, P, and S atoms on the surface. This catalyst had impressive reactivity results, with an HDS conversion of 99%, an HDN conversion of 91%, and an HDO conversion of 80%, and are among the best reported in the literature. These were much higher than those of a commercial catalyst, which gave an HDS conversion of 76% and an HDN conversion of 38%.

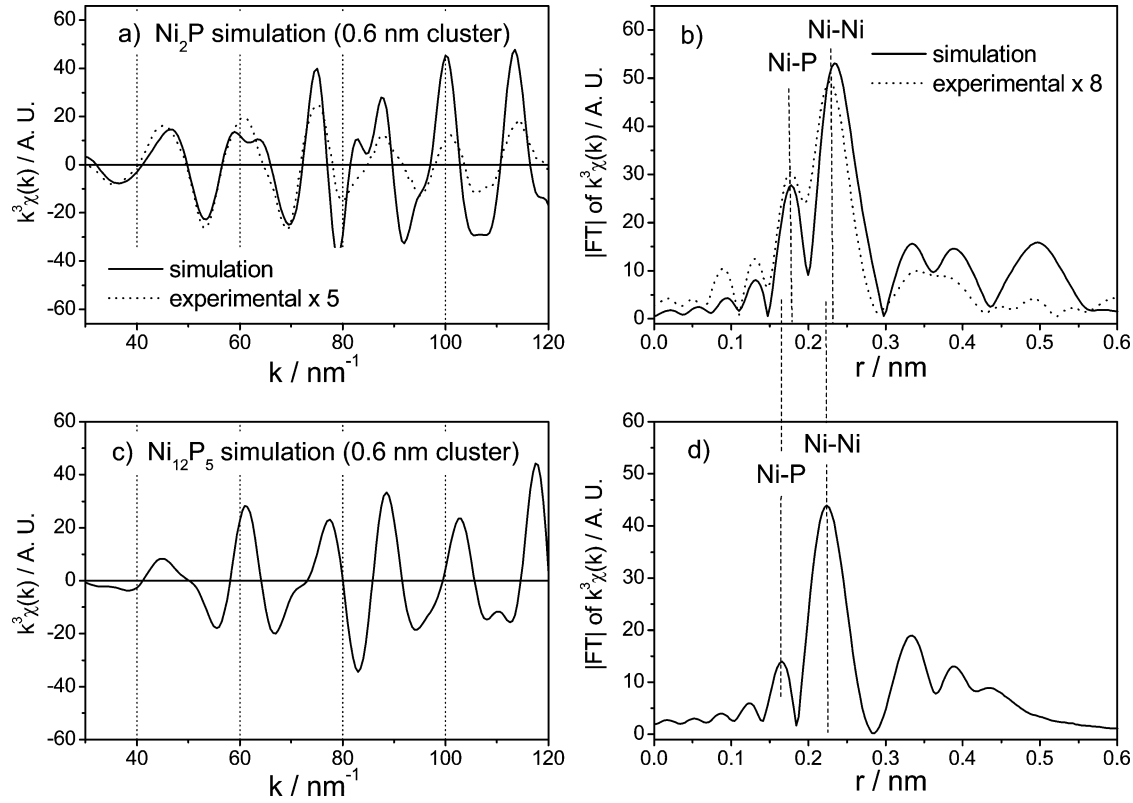

Fig. 10. FEFF simulations for Ni_2P and $Ni_{12}P_5$.

Table 6
Curve-fitting results of Ni K-edge EXAFS for Ni_2P

Sample	Ni–P				Ni–Ni				
	N[a]	R[b] (nm)	σ^2 (10^{-5} nm^2)	ΔE (eV)	N[a]	R[b] (nm)	σ^2 (10^{-5} nm^2)	ΔE (eV)	R_f[f] (%)
Ni_2P[c]	2	0.22662	–	–	4	0.26783	–	–	
$Ni_{12}P_5$[d]	1	0.22294	–	–	2	0.26347	–	–	
Ni_2P (Cerac)[e]	1.809	0.22608	9.63	−1.525	2.312	0.26138	6.42	−1.710	3.3

[a] Coordination number.
[b] Radial distance from the absorber.
[c] Crystallographic data from Ref. [13].
[d] Crystallographic data from Ref. [14].
[e] Curve-fitted by FEFF-simulated function for Ni_2P ($\Delta R = 0.158$–0.258).
[f] $R_f = \frac{\sum_{i=1}^{N} |\chi_{exp}(i) - \chi_{theo}(i)|}{\sum_{i=1}^{N} |\chi_{exp}(i)|} \times 100\%$.

Acknowledgments

We acknowledge support from the US Department of Energy, Office of Basic Energy Sciences, through Grant DE-FG02-963414669, from the NEDO International Joint Research Program. We also appreciate the use of beamline BL12B at the Tsukuba Photon Factory of the High Energy Accelerator Research Organization under Grant 2001G297 and beamline X18B at the National Synchrotron Light Source at Brookhaven National Laboratory under Grant 4513.

References

[1] W. Li, B. Dhandapani, S.T. Oyama, Chem. Lett. 207 (1998).
[2] S.T. Oyama, P. Clark, X. Wang, T. Shido, Y. Iwasawa, S. Hayashi, J.M. Ramallo-Lopez, F.G. Requejo, J. Phys. Chem. B 106 (2002) 1913.
[3] C. Stinner, R. Prins, Th. Weber, J. Catal. 191 (2000) 438.
[4] P. Clark, X. Wang, P. Deck, S.T. Oyama, J. Catal. 210 (2002) 116.
[5] D.C. Phillips, S.J. Sawhill, R. Self, M.E. Bussell, J. Catal. 208 (2002) 456.
[6] S.T. Oyama, J. Catal., in press.
[7] X. Wang, P. Clark, S.T. Oyama, J. Catal. 208 (2002) 321.
[8] C. Stinner, R. Prins, Th. Weber, J. Catal. 202 (1) (2001).
[9] T. Korányi, Appl. Catal. A: Gen. 237 (2002) 1.
[10] S.T. Oyama, X. Wang, Y.K. Lee, K. Bando, F. Requejo, J. Catal. 210 (2002) 207.

[11] S.T. Oyama, X. Wang, F. Requejo, T. Sato, Y. Yoshimura, J. Catal. 209 (2002) 1.
[12] B.D. Cullity, in: Elements of X-Ray Diffraction, 2nd ed., Addison–Wesley, Menlo Park, CA, 1978, p. 102.
[13] A.L. Ankudinov, B. Ravel, J.J. Rehr, S.D. Congradson, Phys. Rev. B 58 (1998) 7565.
[14] E. Larson, Arkiv. Kemi. 23 (1965) 335.
[15] E. Larson, Arkiv. Kemi. 23 (1965) 345.
[16] S. Ramanathan, S.T. Oyama, J. Phys. Chem. 99 (1995) 16365.
[17] S. Rundqvist, Acta Chem. Scand. 16 (1962) 992.
[18] Powder Diffraction Data Files, JCPDS International Center for Diffraction Data, Swathmore, PA, 1992.
[19] S.J. Tauster, T.A. Pecoraro, R.R. Chianelli, J. Catal. 63 (1980) 515.
[20] V. Meille, E. Schulz, M. Lemaire, M. Vrinat, J. Catal. 170 (1997) 29.
[21] F. Bataille, J.L. Lemberton, P. Michaud, G. Pérot, M. Vrinat, M. Lemaire, E. Schulz, M. Breysse, S. Kasztelan, J. Catal. 191 (2000) 409.
[22] M. Boudart, G. Djega-Mariadasson, Kinetics of Heterogeneous Catalytic Reactions, Princeton University Press, Princeton, NJ, 1984.
[23] J.M. Thomas, J.W. Thomas (Eds.), Principles and Practice of Heterogeneous Catalysis, VCH, Weinheim, 1996.